


Regulating positioning and orientation of mitotic spindles via cell size and shape

Jingchen Li and Hongyuan Jiang*

Department of Modern Mechanics, CAS Key Laboratory of Mechanical Behavior and Design of Materials, University of Science and Technology of China, Hefei, Anhui 230027, China (Received 27 June 2017; revised manuscript received 16 September 2017; published 19 January 2018)

Proper location of the mitotic spindle is critical for chromosome segregation and the selection of the cell division plane. However, how mitotic spindles sense cell size and shape to regulate their own position and orientation is still largely unclear. To investigate this question systematically, we used a general model by considering chromosomes, microtubule dynamics, and forces of various molecular motors. Our results show that in cells of various sizes and shapes, spindles can always be centered and oriented along the long axis robustly in the absence of other specified mechanisms. We found that the characteristic time of positioning and orientation processes increases with cell size. Spindles sense the cell size mainly by the cortical force in small cells and by the cytoplasmic force in large cells. In addition to the cell size, the cell shape mainly influences the orientation process. We found that more slender cells have a faster orientation process, and the final orientation is not necessarily along the longest axis but is determined by the radial profile and the symmetry of the cell shape. Finally, our model also reproduces the separation and repositioning of the spindle poles during the anaphase. Therefore, our work provides a general tool for studying the mitotic spindle across the whole mitotic phase.

DOI: [10.1103/PhysRevE.97.012407](https://doi.org/10.1103/PhysRevE.97.012407)**I. INTRODUCTION**

Mitotic spindle, the primary operator of mitosis, is a bipolar assembly of two centrosomes, many microtubules, and associated proteins [1–3]. In general, the mitotic spindle needs a correct and accurate position and orientation in the cell to ensure chromosome segregation and select the cell division plane [4–6], which are essential for conserving genomic information [7], implementing symmetry division [8], and ensuring normal tissue growth and renewal [9]. Therefore, the positioning and orientation of mitotic spindles play a crucial role in cell division.

Many experiments and simulations showed that in the absence of other unspecified mechanisms, the mitotic spindle can be positioned to the cell center, relying on either the pulling force generated by dyneins [10–13] or the pushing force generated by kinesins or microtubule polymerization [14–17]. The combination of pulling forces and pushing forces can provide a more robust mechanism for positioning [18–20]. Similarly, the spindle can also be oriented along the long axis of the cell by the mechanical forces on microtubules [21–23]. However, recent studies suggested that only the pulling force can orient the spindle [21–23]. Whether the pushing force also plays an important role in the orientation process and how it works are still unclear.

In addition to the pushing and pulling forces on microtubules, cell size and shape should also be the key control parameters for the positioning and orientation of mitotic spindles. It has been shown that many interesting phenomena of spindles are regulated by cell size and shape. For instance, experiments found that the spindle size scales with the cell

size only in small cells but approaches an upper limit in large cells [24–26]. When a spherical cell is compressed into a disk shape, the spindle size increases [27,28]. During the metaphase of mitosis, chromosomes aligned on the metaphase plate spontaneously oscillate between the two spindle poles [29], and the period and amplitude of the oscillation increase with the cell size [30]. These examples suggest that cell size and shape may also regulate the positioning and orientation of spindles. However, while many experiments and theories have shown that spindles can be positioned and oriented in various cells effectively [18,19,21–23,31–33], how they are regulated by cell size and shape remains elusive.

In the prevailing models of mitotic spindles, self-assembly, positioning, orientation, and other phenomena were usually studied separately. For example, in most models for positioning [12–14,18,19], the spindle was usually represented by a point, while in the models for orientation [21,22,34], the spindle was assumed to have a fixed shape and size. In these models, only the astral microtubules were considered, but the polar microtubules and kinetochore microtubules were neglected. In contrast, in some computational models for spindle self-assembly [35–37], the interaction between polar microtubules and cross-linkers was considered, but the cortical influence and chromosomes were not taken into account. In the models for spindle size [25,26,38] and chromosome oscillation [39–41], although the polar microtubules, kinetochore microtubules, and chromosomes were considered, the astral microtubules and cell cortex were still ignored. However, the mitotic spindle is a complex structure. Many factors, including the astral microtubules, polar microtubules, various molecular motors, and their interactions with the chromosomes, cortex, and cytoplasm, have indispensable effects on the self-assembly of spindles [3,7,42]. Therefore, a more general model is needed for the study of the mitotic spindle.

*jianghy@ustc.edu.cn

In this paper, we investigate the positioning and orientation of mitotic spindles systematically using a general model that considered the microtubules, various molecular motors, chromosomes, cell shape, and cell size. We find that the microtubule distribution and molecular motors play critical roles in the speed and efficiency of the positioning and orientation processes. We also find that the characteristic time of the positioning and orientation processes increased with cell size, and the characteristic time of orientation process decreased with the aspect ratio of the elliptical cells. Interestingly, in cells of various shapes, the stable spindle orientation is determined by the symmetry and radial profile of the cell shape rather than the longest axis. Finally, our model can be used to investigate the separation and repositioning of spindle poles with the change of cell shape during mitotic anaphase.

II. MODEL AND METHODS

The positioning and orientation of mitotic spindles are investigated using a two-dimensional computational model [28]. As shown in Fig. 1, the mitotic spindle has two centrosomes, several chromosomes, large numbers of microtubules, and various molecular motors. In the following sections, the dynamics of microtubules, molecular motors, centrosomes, and chromosomes will be described systematically.

A. Microtubule dynamics

In general, the mitotic spindle has two centrosomes, several chromosomes, large numbers of microtubules, and various molecular motors (Fig. 1). Most microtubules are nucleated from centrosomes, the microtubule organizing center in the mitotic spindle, and grow radially with their minus ends anchored [3]. We assume that the nucleation rate of microtubules from each centrosome is k_0 and the growth direction of each microtubule was random. Microtubules can also be nucleated from existing microtubules as branches. Considering that branching microtubules have the same polarity as mother microtubules, and the forces on branching microtubules can be transmitted to the centrosome to drive its motion [43,44], we ignore the branches here and assume that all microtubules are nucleated from centrosomes.

Microtubules can randomly switch between growing and shrinking states, which is called the dynamic instability [45]. We define that microtubules grow at a speed of v_1 , and shrink at a speed of v_2 . And the rescue rate (from shrinking to growing) and catastrophe rate (from growing to shrinking) of microtubules are defined as k_1 and k_2 , respectively. These four parameters completely describe the dynamics of free microtubules, and all of them are assumed to be constant in the cytoplasm.

When the growing microtubule contacts a barrier, such as the cortex or chromosomes, it will generate a pushing force on the barrier due to its polymerization [14,45] (Fig. 1). Microtubules can be buckled easily because they are highly slender [46,47]. The critical force of buckling is given as $f_c = \pi^2 \kappa / l^2$ [14,19], where l denotes the length of the microtubule. We assume that the pushing force is constant and equals the critical force when the microtubule is buckled [19,31]. When the stall force f_{stall} is less than the buckling force f_c , the pushing force equals f_{stall} and buckling does not occur. Therefore, the pushing force on the i th microtubule is

$$f_i^* = \min(f_{stall}, \pi^2 \kappa / l_i^2). \tag{1}$$

It is noted that most microtubules are buckled, and thus the pushing force here is naturally length dependent.

In addition, experiments showed that due to the pushing forces, the microtubules can slip along the cortex [31] (Fig. 1). Here we assume that the microtubules can also slip along the chromosome arms. The slipping speed of the microtubule tip is given by [19]

$$v_s = (f_i^* \sin \beta) / \xi. \tag{2}$$

Here ξ is the friction coefficient and β is the angle between the microtubule and the normal to the cortex or chromosome. The slipping behavior breaks the uniformity of the microtubule distribution [19].

B. Molecular motor dynamics

Molecular motors are also essential for the spindle assembly [48,49]. They can consume the energy from the hydrolysis of adenosine triphosphate (ATP) to actively walk along the microtubules [40]. If the motors are also bound to other objects, such as the cortex or chromosome, then they can apply forces on the microtubules (Fig. 1). Motors have different directions of spontaneous walking and thus can generate varying forces.

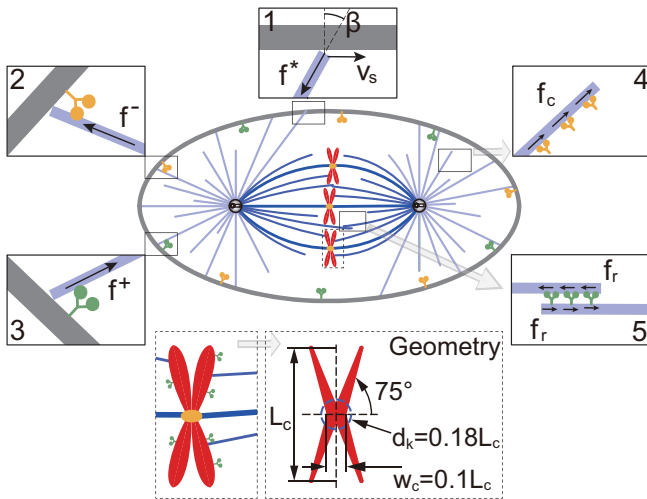


FIG. 1. Schematic diagram of the mechanical model. The schematic diagram of the mitotic spindle is shown at the center, and five force-generation mechanisms are illustrated, including (1) the pushing force generated by hindering the microtubule polymerization, (2) the pulling force generated by cortical dyneins or kinetochores, (3) the pushing force generated by cortical kinesins or chromosome kinesins, (4) the pulling force generated by cytoplasmic dyneins, and (5) the pushing force generated by cross-linkers. Bottom: Chromosomes are assumed as an X-shaped rigid body with a tilt angle 75° of the chromosome arms. The length of the chromosome is L_c . The width of the chromosome is defined as $W_c = 0.1L_c$. The size of the kinetochore is defined as a circle with a diameter of $d_k = 0.18L_c$ (red dot), where the microtubule tips can be bound by the kinetochore.

For example, dynein can walk to the minus end of the microtubules and generate a pulling force, while kinesin can walk to the plus end of the microtubules and generate a pushing force [40]. In our model, both dynein and kinesin are considered, and the superscripts + and - are used to indicate the kinesin and dynein, respectively. The force generated by the motor is velocity dependent as [50,51]

$$f^\pm = f_0^\pm \left(1 - \frac{v^\pm}{v_0^\pm}\right), \quad (3)$$

where f^\pm is the force on the motor, v^\pm is the walking velocity of the motor, f_0^\pm is the stall force of the motor, and v_0^\pm is the unloaded velocity of the motor.

Molecular motors can randomly bind to and unbind from microtubules. The unbinding rate (k_u^\pm) is dependent only on the load applied on the motor as [39]

$$k_u^\pm = k_0^\pm e^{f^\pm/f_u^\pm}, \quad (4)$$

where k_0^\pm is the unloaded unbinding rate, f^\pm is the load on the motor, and f_u^\pm represents the sensitivity of the unbinding rate to the load. In contrast, the binding rate is usually expected to be proportional to the density of the unbound motors. Here we consider the motors at the cortex [19], chromosomes [39,40], cytoplasm [11,52], and those serving as the cross-linkers on the antiparallel microtubules [7,37].

The binding rates of cortical dyneins and kinesins (k_b^\pm) are both assumed constant if we assume the density of the motors on the cortex is uniform. To simplify the computation and make each microtubule contribute equally, we assume each microtubule can be bound by only one cortical motor [19,28,31].

The binding rates of cortical dyneins and kinesins (k_b^\pm) are both assumed constant if we assume the density of the motors on the cortex is uniform. To simplify the computation and make each microtubule contribute equally, we assume each microtubule can be bound by only one cortical motor [19,28,31].

Molecular motors also distribute on the chromosome and can bind to the microtubules [39] (Fig. 1). For example, chromokinesins can be bound to the microtubules and apply a pushing force on the microtubules as well as the chromosome arms. [39,40]. The binding rate of the kinesins on the arms is represented by $k_{b,c}^+$. We also assume that each microtubule can be bound only by one chromokinesin on the arm, and the force follows the same rule as the cortical kinesin. In contrast, the central kinetochore region is under tension, which is generated by the microtubule depolymerization [53]. We define the binding rate of kinetochores as $k_{b,c}^-$, and the force generated here is assumed to be the same as that of dyneins.

The pulling force generated by the dyneins that are carrying cargoes in the cytoplasm is also important for the positioning of the spindles [11,52,54] (Fig. 1). This force is dependent on the microtubule length because a longer microtubule can be bound by more motors. Therefore, we simply assume this cytoplasmic pulling force on the i th microtubule is $f_{c,i} = \eta l_i$, where η is the force per unit microtubule length and l_i is the length of the microtubule.

Cytoplasmic motors can also bind to a pair of antiparallel microtubules to serve as cross-linkers [7] (Fig. 1). These motors can also walk actively and generate pushing forces on the antiparallel microtubules, which plays an important role in maintaining the spindle length [37,55,56]. However, in the two-dimensional (2D) model, the microtubules can hardly bypass the chromosomes to form the antiparallel structure. In our recent work, we developed a model without chromosomes

to calculate the force generated only by the cross-linkers on the spindle poles [28]. The results can be fitted by $f_r = A e^{-BL_s}$, where $A = 360$ pN and $B = 0.08 \mu\text{m}^{-1}$ are constants and L_s is the pole-to-pole distance, that is, the spindle length. Therefore, we superpose this force in the model and no longer explicitly consider the cross-linkers.

C. Centrosome and chromosome dynamics

The forces applied on the microtubules can all be transferred to the centrosome. We assume the two centrosomes as two particles due to their small size. If the inertial forces are neglected because of the low Reynolds number, then the kinetic equation of a centrosome can be given by

$$\sum_{i \in O} f_{c,i} \vec{m}_i + \sum_{i \in P} f_i^* \vec{m}_i + \sum_{i \in Q} f_i \vec{m}_i + \vec{f}_r + \sum_{\beta \in R} \vec{f}_d^{\alpha\beta} + \xi_p \vec{v}_p = 0, \quad (5)$$

where O is the set of microtubules nucleated from this centrosome, P is the subset of O slipping on the cell cortex or chromosomes, Q is the subset of O bound by the motors on the cortex or chromosomes, \vec{m}_i is the unit vector along the direction of the i th microtubule, ξ_p is the viscous drag coefficient of the centrosome in the cytoplasm, and \vec{v}_p is the velocity of the centrosome. In Eq. (5), the first four items represent the forces from the above-mentioned mechanisms, and the last item is the viscous drag force. The fifth item represents the limitation that the chromosomes and centrosomes cannot overlap with each other or penetrate the cortex. This limitation is defined as a short-range repulsive force, $f_d^{\alpha\beta} = C/d_{\alpha\beta}$ for $d_{\alpha\beta} < 1 \mu\text{m}$, where $C = 200 \text{ N } \mu\text{m}$ is a constant and $d_{\alpha\beta}$ is the minimum distance between two objects, including the cortex, centrosomes, and chromosomes. In the fifth item of Eq. (5), the index α represents the considered centrosome and R includes the other centrosome, all chromosomes, and the cell cortex.

The chromosomes are assumed as X-shaped rigid bodies (Fig. 1) based on some experimental observations [63–65]. The kinetic equations of a chromosome are given by

$$\sum_{i \in M} f_i^* \vec{m}_i + \sum_{i \in N} f_i \vec{m}_i + \sum_{\beta \in H} \vec{f}_d^{\alpha\beta} + \xi_c \vec{v}_c = 0 \quad (6)$$

and

$$\sum_{i \in M} (\vec{r}_i \times f_i^* \vec{m}_i) + \sum_{i \in N} (\vec{r}_i \times f_i \vec{m}_i) + \zeta_c \dot{\alpha}_c = 0, \quad (7)$$

where M is the subset of the microtubules slipping on the chromosome; N is the subset of the microtubules bound by motors or kinetochores on the chromosome; \vec{r}_i is the vector pointing from the chromosome center to the point of force application; ξ_c and ζ_c are the translational and rotational viscous drag coefficients of the chromosome, respectively; \vec{v}_c is the centroid velocity of the chromosome; and α_c is the orientation angle of the chromosome. The index α represents the chromosome considered in Eq. (6), and H includes the other chromosomes, two centrosomes, and the cortex. In addition, for simplicity, the efficient frontier of the chromosome is defined as its circumference, and thus the antioverlapping force $f_d^{\alpha\beta}$ applies no torque on the chromosome.

D. Stochastic simulation method

Stochastic simulations are performed in MATLAB to reproduce the movement of the mitotic spindles in various cells [28]. To investigate the orientation of the mitotic spindles, we assume the cell has a long axis. In experiments, most cells round up on mitosis. However, because of the stress applied by other cells in the tissue, round cells in the tissue might be stretched to an elliptical shape [33,66]. Therefore, the 2D cell in the simulation is initially assumed to be an ellipse with a long axis of $30 \mu\text{m}$ and a short axis of $15 \mu\text{m}$. The parameters used in the simulations are summarized in Table S1 in the Supplemental Material [57] unless otherwise specified.

In the simulation, we record the length, direction, and state of every microtubule. Each microtubule has four states, including growing, shrinking, slipping, and binding, and they can switch from one to another. In detail, if the microtubule has not touched the cortex or chromosomes, then it can switch between the growing and shrinking states through catastrophe or rescue. If the growing microtubule touches the cortex or chromosomes, then it will switch to the slipping state. The slipping microtubule can switch to the shrinking state through catastrophe, or switch to the binding state after the binding of a motor. If the motor unbinds, then the binding microtubule will switch to the shrinking state. If the shrinking

microtubule completely depolymerizes, then the microtubule will be deleted. The length and direction of the microtubules change according to their states. Specifically, the growing and shrinking microtubules only change their length according to the velocity v_1 and v_2 . The slipping microtubules change their direction according to the slipping speed [Eq. (2)]. The binding microtubules keep their tips fixed on the cortex or chromosomes.

Initially, we randomly give the positions of the centrosomes and chromosomes in the cell. In each time step, new microtubules are nucleated in random directions. For each microtubule, first we determine whether the microtubule switches its state randomly or determinately. The random switchings include catastrophe, rescue, binding, and unbinding. Each event has a corresponding rate. We can calculate the probability of the random events in a time step. A uniformly random number in $(0, 1)$ is generated, and if it is less than the probability, random switching will occur. Second, the length and direction change deterministically according to the microtubule state. Third, the force generated by every microtubule can be calculated based on its length, direction, and state [Eqs. (1) and (3)]. Therefore, the resultant force on each centrosome and chromosome can be calculated to obtain their instantaneous velocity and new position [Eqs. (5)–(7)]. The system is iteratively solved.

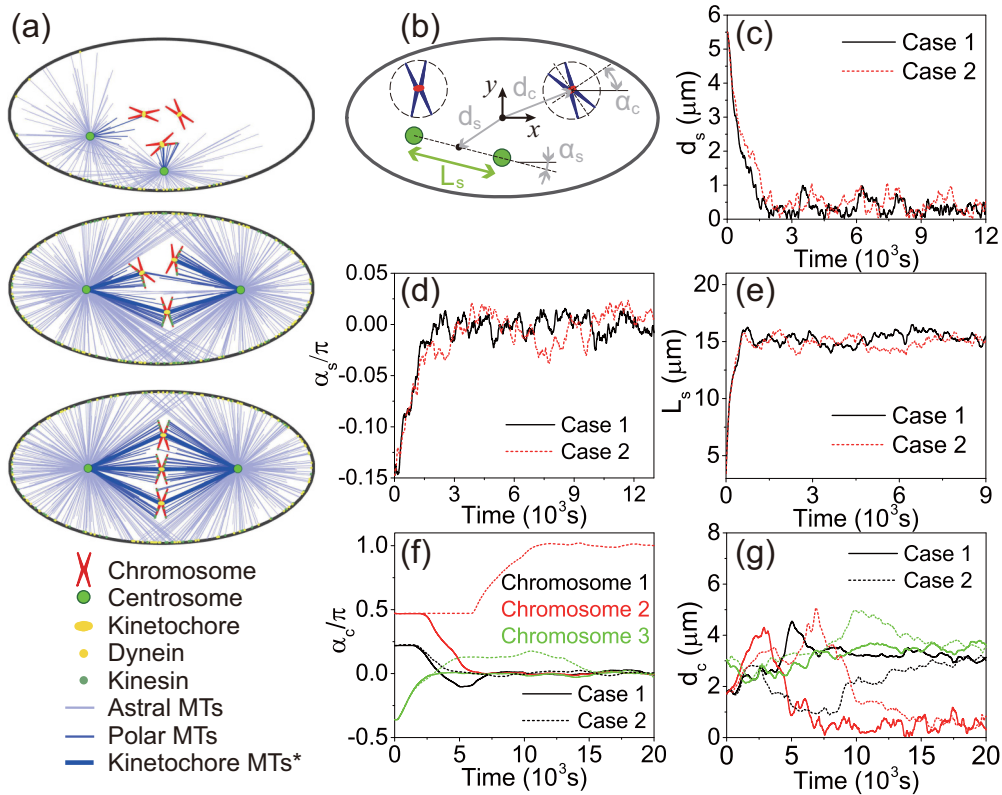


FIG. 2. Self-assembly, positioning, and orientation of the mitotic spindle with three chromosomes and two centrosomes. (a) Screenshots of the simulation (see also Movie 1 in the Supplemental Material [57]). Initially, the centrosomes are located at $(-5, -3.5)$ and $(-2, -5)$; the chromosomes are located at $(1.7, 0)$, $(-1.7, 0)$, and $(0, -3)$; and their orientations are 2.26 rad , 3.05 rad , and 0.44 rad . *The line width represents the number of microtubules overlapping at the kinetochore. (b) The schematic diagram illustrates the indicators of the spindle position d_s , spindle orientation α_s , spindle length L_s , chromosome position d_c , and chromosome orientation α_c . Two examples (solid lines and dashes, respectively) show the time evolution of the (c) spindle position, (d) spindle orientation, (e) spindle length, (f) chromosome orientation, and (g) chromosome position with the same initial conditions.

III. RESULTS

A. Self-assembly, positioning, and orientation of mitotic spindle

We first simulate the self-assembly, positioning, and orientation of the mitotic spindle with three chromosomes and two centrosomes in an elliptical cell (Fig. 2 and Movie 1 in the Supplemental Material [57]). During the self-assembly process, first the centrosomes are separated and positioned at two sides of the chromosomes. Then the microtubules search and attach the kinetochores and gradually align the chromosomes onto the equatorial plate [Fig. 2(a)]. Further, the position d_s and orientation α_s of the spindle defined in Fig. 2(b) both approach and fluctuate around zero [Figs. 2(c) and 2(d)], which indicates that the spindle is positioned at the cell center and oriented along the long axis of the cell. The spindle length, that is, the pole-to-pole distance, also approaches a stable value as the spindle is positioned and oriented [Fig. 2(e)].

In order to investigate the positioning and orientation of the spindles, we need to quantify the process properly and reduce unnecessary computational costs. First, we note that the positioning and orientation can be accomplished in advance of aligning chromosomes onto the equatorial plane [Figs. 2(c)–2(g)]. Considering that the aligning process is slow and complex, we simplify it by using one chromosome magnified by 3 times to replace the three chromosomes. In this way, the positioning and orientation of the spindle are almost unchanged [Figs. 3(a)–3(c)], but the computational efficiency is significantly improved since the degrees of freedom are reduced. Second, we note that the chromosomes can be aligned through different stochastic paths, for example, the two cases in Fig. 2. Even if the number of chromosomes is reduced to 1, the centrosomes can still be positioned through different paths (Fig. S1 and Movie 2 in the Supplemental Material [57]). If the two centrosomes are initially positioned on the two sides of the chromosome, then the multipath phenomenon can be avoided (Figs. 3(b) and 3(c) and Movie 3 in the Supplemental Material [57]). Interestingly, wherever the initial positions of centrosomes and chromosomes are, the spindle can always be self-assembled, positioned, and oriented [Figs. 3(d) and 3(e)], which indicates the robustness of the model.

We find that the position d_s and orientation α_s of the spindle both approach zero exponentially [Figs. 3(b) and 3(c)], which is in agreement with the experimental observations of the positioning of one microtubule organizing center [67] and the orientation of the *in vivo* spindles [68] qualitatively. Thus we can fit the curves by using exponential functions to obtain the characteristic time, τ_d and τ_α , which can be used to quantify the required time of the positioning and orientation processes [Figs. 3(b) and 3(c)]. Therefore, a general model is obtained to investigate how the positioning and orientation of the spindles are regulated by cell size, shape, and other control parameters.

B. Forces on microtubules influence the positioning and orientation of spindles

The forces generated by the cell cortex play an essential role in the positioning and orientation of mitotic spindles [4,5,21]. We then focus on the microtubules associated with the cortex and explore the influence of the number, distribution,

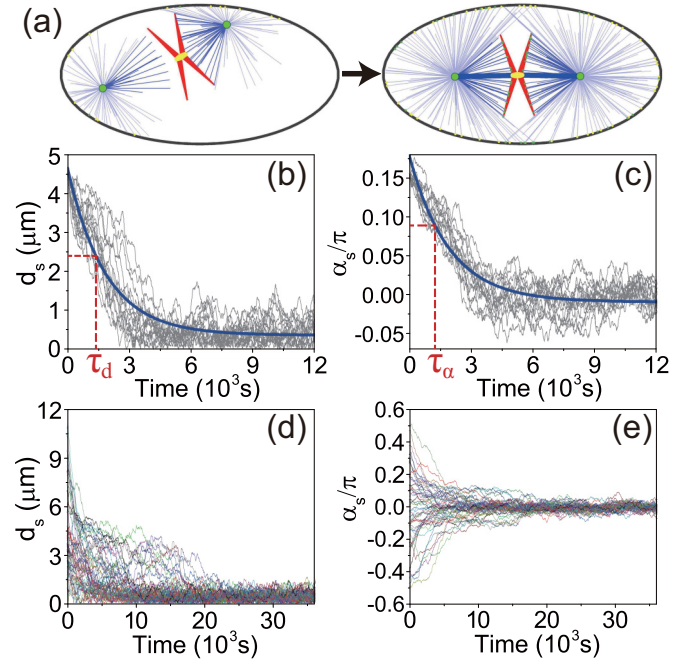


FIG. 3. Self-assembly, positioning, and orientation of the mitotic spindle with two centrosomes and one chromosome. (a) Screenshots of the simulation at the beginning and end (see also Movie 3 in the Supplemental Material [57]). Initially, the two centrosomes are located at $(-10.2, -1.3)$ and $(2.2, 5.3)$, the chromosome is located at $(-2, 2)$, and its orientation is 0.5 rad. The time evolution of the (b) spindle position and (c) orientation (20 simulations) is shown, which can be fitted by $d_s = ae^{-t/\tau_d}$ and $\alpha_s = be^{-t/\tau_\alpha}$ (blue thick line) to obtain the characteristic time, τ_d and τ_α (red dashed). From 100 groups of random initial conditions, the spindles can always be (d) positioned at the cell center and (e) oriented along the long axis of the cell.

and composition of the microtubules on the positioning and orientation processes.

First, the number of microtubules can be changed by the nucleation rate and the parameters of the microtubule dynamics. For example, as the nucleation rate increases, the amount of microtubules increases. More microtubules can generate larger forces on the spindle and obviously accelerate the spindle's movement. Therefore, increasing the total number of microtubules can decrease the characteristic time of positioning and orientation processes [Fig. 4(a)].

Second, the spatial distribution of the microtubules is mainly determined by their slipping [19]. The nonuniformity of the microtubule distribution increases with the slipping speed, which in turn is inversely proportional to the drag coefficient ξ . Therefore, we can control the spatial distribution of the microtubules by ξ .

Third, we define the composition of the microtubules as the proportion of pulling microtubules in the cortical microtubules. There are three kinds of microtubules associated with the cortex, including those slipping on the cortex, captured by the cortical kinesins, and captured by the cortical dyneins. Their numbers follow the continuity equations

$$\frac{dN^\pm}{dt} = k_b^\pm N^* - k_u^\pm N^\pm, \quad (8)$$

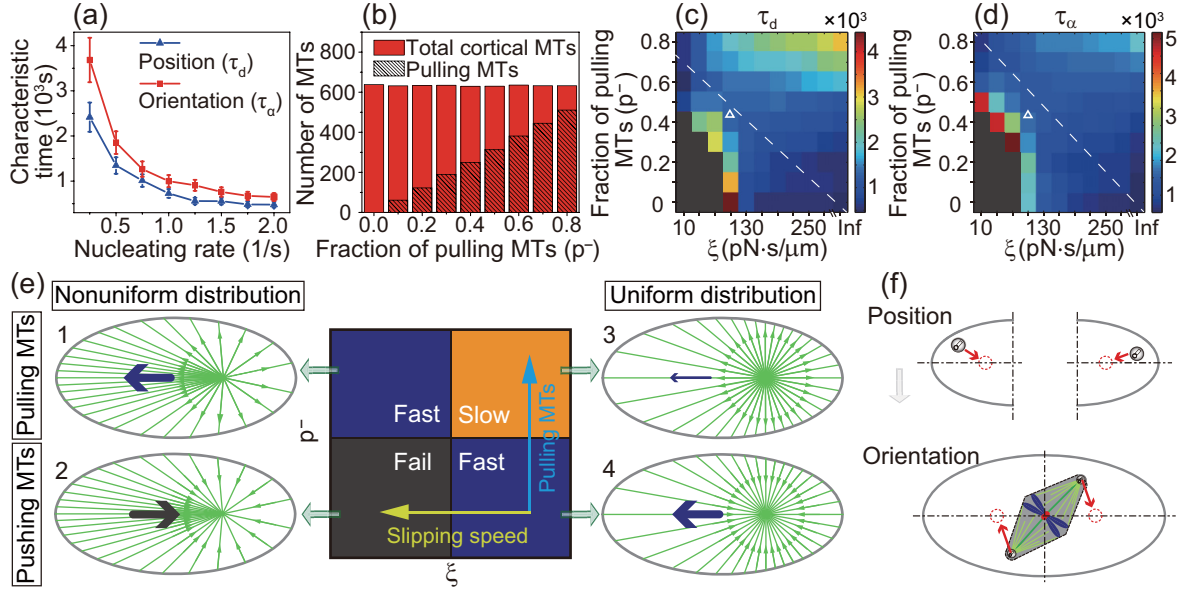


FIG. 4. Influence of the number, distribution, and composition of cortical microtubules on the positioning and orientation of mitotic spindles. (a) The characteristic time of the positioning and orientation vs. the nucleating rate (mean \pm SE from 20 simulations). (b) The time-averaged numbers of the total cortical microtubules and the pulling cortical microtubules with the various fraction of the pulling microtubules, p^- , which is changed by the binding rate of dynein, k_b^- . The characteristic time of (c) positioning and (d) orientation are the functions of the fraction of the pulling microtubules, p^- , and the slipping drag coefficient, ξ , obtained by averaging 50 simulations for each case. The triangle indicates the values used in other sections. The white dash marks the cases that are most efficient. The black area in the lower left corner means the process is failed. The other settings are the same as those used in Fig. 3(a). (e) The schematic of the positioning mechanism. The results in (c) can be summarized as four regimes, relying on the slipping speed and the major force on the microtubules. The green arrows on the microtubules (four insets) indicate the major force (pulling or pushing). The big arrows (four insets) indicate the total force on the spindle. (f) Positioning the two poles, respectively, can provide a torque to orient the spindle.

where N^* is the number of microtubules slipping on the cortex, N^\pm is the number of microtubules captured by the cortical kinesins (+) and dyneins (-), and k_b^\pm and k_u^\pm are the binding and unbinding rates of the motors, respectively. We define the fraction of pulling microtubules as $p^- = N^- / (N^+ + N^- + N^*)$ to quantify the composition of the microtubules. Here $(N^+ + N^- + N^*)$ is the total number of cortical microtubules. At the stable state ($dN^\pm/dt = 0$), the fraction of pulling microtubules can be derived as

$$p^- = \frac{k_u^+ k_b^-}{k_u^+ k_b^- + k_u^- k_b^+ + k_u^+ k_u^-}. \quad (9)$$

Equation (9) shows that the fraction of pulling microtubules at the stable state is determined by the four parameters, the binding and unbinding rates of cortical kinesins and dyneins. We can regulate the fraction of pulling microtubules p^- in the range of $\sim 0-0.8$ through changing the binding rate of cortical dyneins k_b^- in the range of $\sim 0-0.16$, keeping the other three parameters unchanged. In the simulations with different values of p^- , we can obtain the corresponding fraction of the pulling cortical microtubules as shown in Fig. 4(b). Therefore, we can control the composition of the cortical microtubules effectively.

The characteristic time of the positioning and orientation processes with different fractions of pulling microtubules (p^-) and drag coefficients (ξ) is shown in Figs. 4(c) and 4(d). We find that along the dashed lines (the region where the slipping drag coefficient positively correlates to the fraction of the pulling microtubules), the positioning and orientation

can be accomplished quickly and efficiently. In the upper right corner, the positioning and orientation processes will slow down with an increase in the pulling microtubules or the drag coefficient. This is in agreement with the experiment results that the positioning of the spindles becomes weaker with the activation of the cortical dyneins [69]. Finally, in the lower left corner, that is, in cases of low pulling force and high slipping speed, the spindles fail to position and orient themselves.

This result is summarized in Fig. 4(e). It should be noted that the microtubules are randomly nucleated from the centrosomes, so the microtubules approximate a uniform distribution if the slipping speed is low [insets 3 and 4 of Fig. 4(e)]. In this case, if p^- is low, that is, if the pushing microtubules are dominant, then the spindle is quickly positioned because the pushing force generated by the shorter microtubules is larger and can drive the spindle to the cell center [inset 4 of Fig. 4(e)]. But if the pulling microtubules are dominant (p^- is high), then the positioning process is slow since the pulling force is length independent [inset 3 of Fig. 4(e)]. However, with an increase in the slipping speed, more microtubules slip to one side and have larger lengths [insets 1 and 2 of Fig. 4(e)]. In this case, if the pulling microtubules are dominant, then the spindle can be pulled to the cell center [inset 1 of Fig. 4(e)]. However, if the pushing microtubules are dominant, then the spindle will be pushed to the cell boundary [inset 2 of Fig. 4(e)]. Therefore, the proper distribution and composition of the microtubules can provide a fast and efficient positioning process.

The influence of microtubules on the orientation and positioning processes is similar [Figs. 4(c) and 4(d)], which

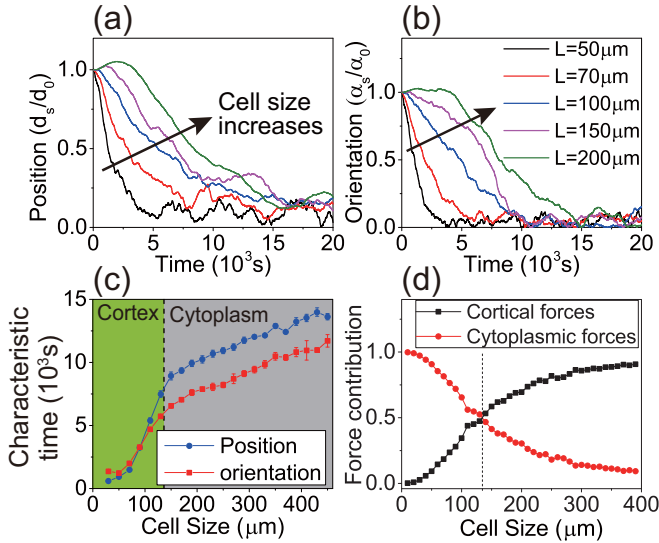


FIG. 5. The influence of cell size on the positioning and orientation of the spindles. The (a) position and (b) orientation of the mitotic spindles [indicated by d_s and α_s defined in Fig. 2(b)] in cells of various sizes are plotted as functions of time. Both the position and orientation are normalized by their initial values. (c) Characteristic time of the positioning and orientation vs. the cell size (mean \pm SE from 50 simulations). (d) The contribution of cortical and cytoplasmic forces to the total force which drives the spindle motion in cells of various sizes (averaged over time for each case). The transition point is around $135 \mu\text{m}$ (dashed line) with our parameters, corresponding to that in (c).

indicates that the positioning and orientation of the spindles have the same mechanism. It has been shown that the spindle is positioned to the cell center by the forces on the microtubules. However, the forces on the spindles are actually applied on the two spindle poles. The forces that position the two poles can provide a torque on the spindle and drive its orientation process [Fig. 4(f)]. Therefore, the positioning and orientation occur simultaneously and rely on both the pushing force and pulling force.

C. Cell size influences the positioning and orientation of spindles

Next, we investigate how the cell size influences the positioning and orientation of mitotic spindles. Living cells are usually several microns to hundreds of microns in size during the early embryogenesis [24,52]. We change the cell size in this range and keep the cell shape and the other settings consistent with the simulations in Fig. 3(a). As expected, the characteristic time of the positioning and orientation processes increases with the cell size [Figs. 5(a) and 5(b)], which indicates that the smaller cell can provide larger driving forces of positioning and orientation. This is in agreement with the experimental results [69].

Interestingly, we find that the characteristic time of positioning and orientation increases fast in small cells but slowly in large cells [Fig. 5(c)], which indicates that there are probably two different control mechanisms. It has been shown that the force generated by the cortical microtubules can position and orient the spindle inside the cell (Fig. 4). It should be

noted that another length-dependent force, the pulling force generated by the cytoplasmic motors [52,54], can also act as the position sensor and drive the positioning and orientation of the spindle. The cortical force decreases with the cell size because there are fewer microtubules contacting the cortex in larger cells. In contrast, the cytoplasmic force increases with cell size because the microtubules can be longer in larger cells. Therefore, in large cells, the cytoplasmic pulling force should be more important for the positioning and orientation. To test this idea, we calculate the contribution of the two types of forces to the total force on the spindle. It indeed shows that in small cells, the cortical force plays a dominant role, while in large cells, the cytoplasmic force dominates [Fig. 5(d)].

Taken together, we conclude that the spindle is positioned and oriented mainly by the cortical force in the small cells and by the cytoplasmic force in the large cells. The mechanism of the cortical force leads to the fast increase law of the characteristic time in the small cells, while the mechanism of the cytoplasmic force results in the slow increase law in the large cells [Fig. 5(c)].

D. Cell shape influences the positioning and orientation of spindles

It has been proposed that the spindle orientation is mainly determined by the aspect ratio of the cells [23,32,33,66]. We define the aspect ratio of an elliptical cell as λ_0 ($\lambda_0 \geq 1$) [Fig. 6(a)]. When $\lambda_0 = 1$, the cell is round. The cell becomes more slender with λ_0 . We keep the cell area (or the cell volume in 3D) constant but change the aspect ratio λ_0 in the simulations. We find that the characteristic time of the orientation process decreases exponentially with the aspect ratio [Fig. 6(a)]. In contrast, the characteristic time of positioning increases slightly. The positioning process becomes slower because the cell length increases with the aspect ratio due to the constant cell area. However, since the cell width decreases with the aspect ratio, the resultant torque on the spindle increases, which results in a faster orientation process [Fig. 6(a)]. Therefore, in the experiments of Ref. [21,23], although the expectation of the spindle orientation is along the long axis, the more slender cell generates the smaller torque on the spindle, which results in the increase of the orientation deviation.

However, the aspect ratio is only one important aspect of the cell shape. Some complex shapes cannot be described by the aspect ratio alone. For example, cells usually are polygonal in the epithelial tissue [23,32,66]. Polygonal cells can also be obtained under confinement in the microfabricated chambers [21,70,71] or the extracellular matrix [9,22,72]. The cell shape will remain polygonal during the metaphase if mitotic cell rounding is inhibited by the limited space [21] or some proteins [73–75]. Therefore, an essential question is how cells select the spindle orientation in such polygonal cells.

To answer this question, we provide the initial positions of the chromosomes and centrosomes randomly in various polygonal cells and observe the spindle orientation in the stable state. As expected, the probability distribution of the stable spindle orientation has several peaks in the pentagonal and hexagonal cells, corresponding to their diagonal lines [Figs. 6(c) and 6(d)]. Anomalously, the spindle orientation approximates a

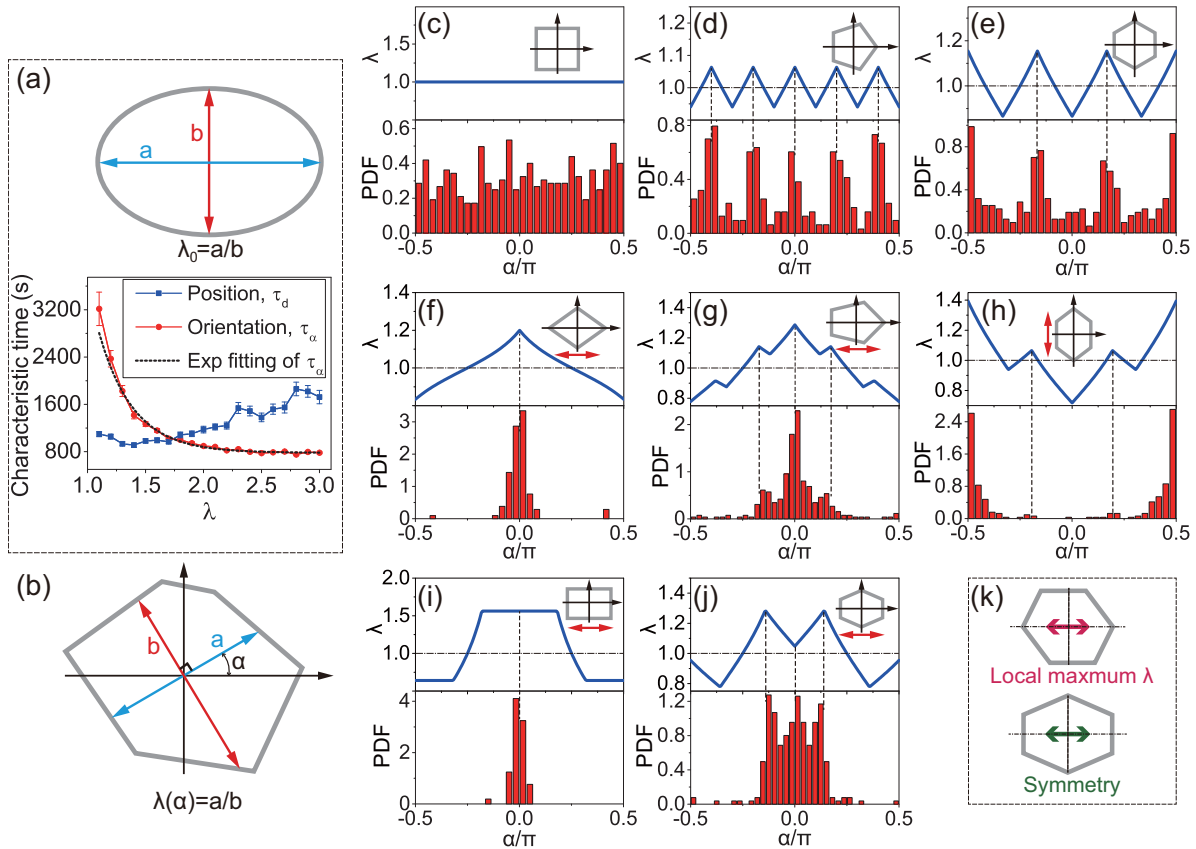


FIG. 6. The influence the of cell shape on the positioning and orientation of the spindles. (a) Top:) The schematic diagram of the aspect ratio of elliptical cells, λ_0 . Bottom: The characteristic time of positioning and orientation vs. the aspect ratio λ_0 of elliptical cells (mean \pm SE from 50 simulations). The other settings are the same as those used in Fig. 3(a). The curve of τ_α can be fitted by an exponential decay function (black dashed curve). (b) The schematic diagrams of the radial profile of elliptical cells, $\lambda(\alpha)$. [(c)–(j)] The cellular radial profile λ and the probability density function (PDF) of the stable spindle orientation are the functions of angle α in various elliptical cells. The stable spindle orientations are obtained from the simulations that 100 initial positions of centrosomes and chromosomes are given randomly. Here, we consider eight shapes, including [(c)–(e)] three equilateral polygons and [(f)–(j)] elongated along different directions. The red double arrows indicate the elongation direction. (k) The two selections of the stable spindle orientation in elliptical cells, the local maximum λ , and the symmetric axis.

uniform distribution in the square cells [Fig. 6(c)]. Inspired by the definition of the aspect ratio of elliptical cells, we define the radial profile of the polygon, $\lambda(\alpha)$, as shown in Fig. 6(b). We find the radial profile of square cells is constant [Fig. 6(c)], while the radial profile of pentagonal and hexagonal cells has several peaks corresponding to their diagonal lines [Figs. 6(d) and 6(e)]. This is in good agreement with the probability distribution of the stable orientation in these regular polygons. For more insight, we change λ by elongating the square and hexagonal cells slightly along their diagonal line and elongating the pentagonal cells along its symmetric axis [Figs. 6(f)–6(h)]. We find that the spindles still tend to be oriented along the direction with a local maximum of λ and $\lambda > 1$ [Figs. 6(f)–6(h)]. We also find that the spindle has a larger probability to orient along the direction with the higher peak value of λ [Figs. 6(g) and 6(h)].

In addition, we noted that the radial profile λ of the rectangular cells has a platform with a maximum value [Fig. 6(i)], but the spindle tends to be oriented along the symmetric axis. Similarly, in the hexagonal cells elongated along another axis, the spindle tends to be oriented along either the peaks of λ or the long symmetry axis of the cell [Fig. 6(j)]. Therefore,

we propose a rule that the final spindle orientation is most possibly along the local maximum of λ ($\lambda > 1$) or the long symmetric axis [Fig. 6(k)]. If the peak value of λ is bigger, then the probability that the spindle is along this direction can be larger.

If the rule is generally applicable, then we can predict the spindle orientation in other shapes. This method can be more convenient, quick, and intuitive than the time-consuming simulations. To test this rule, we compare the rule-based predictions to the available experiment data in Ref. [21]. The simulation results of the spindle orientation in square cells and rectangular cells are in good agreement with the experimental results. Thus, we only compare the other experiment data.

As shown in Fig. 7, based on the rule of the spindle orientation [Fig. 6(k)], we first plot the radial profile λ of each cell shape in the polar coordinate system. It should be noted that the experimental results showed the division-axis orientation but not the spindle orientation. In general, these two orientations in one cell are orthogonal. Therefore, we rotate the radial profile 90° to indicate the division-axis orientation (blue line). As predicted, the experiments results show a clear preference of division-axis orientation at each local maximum

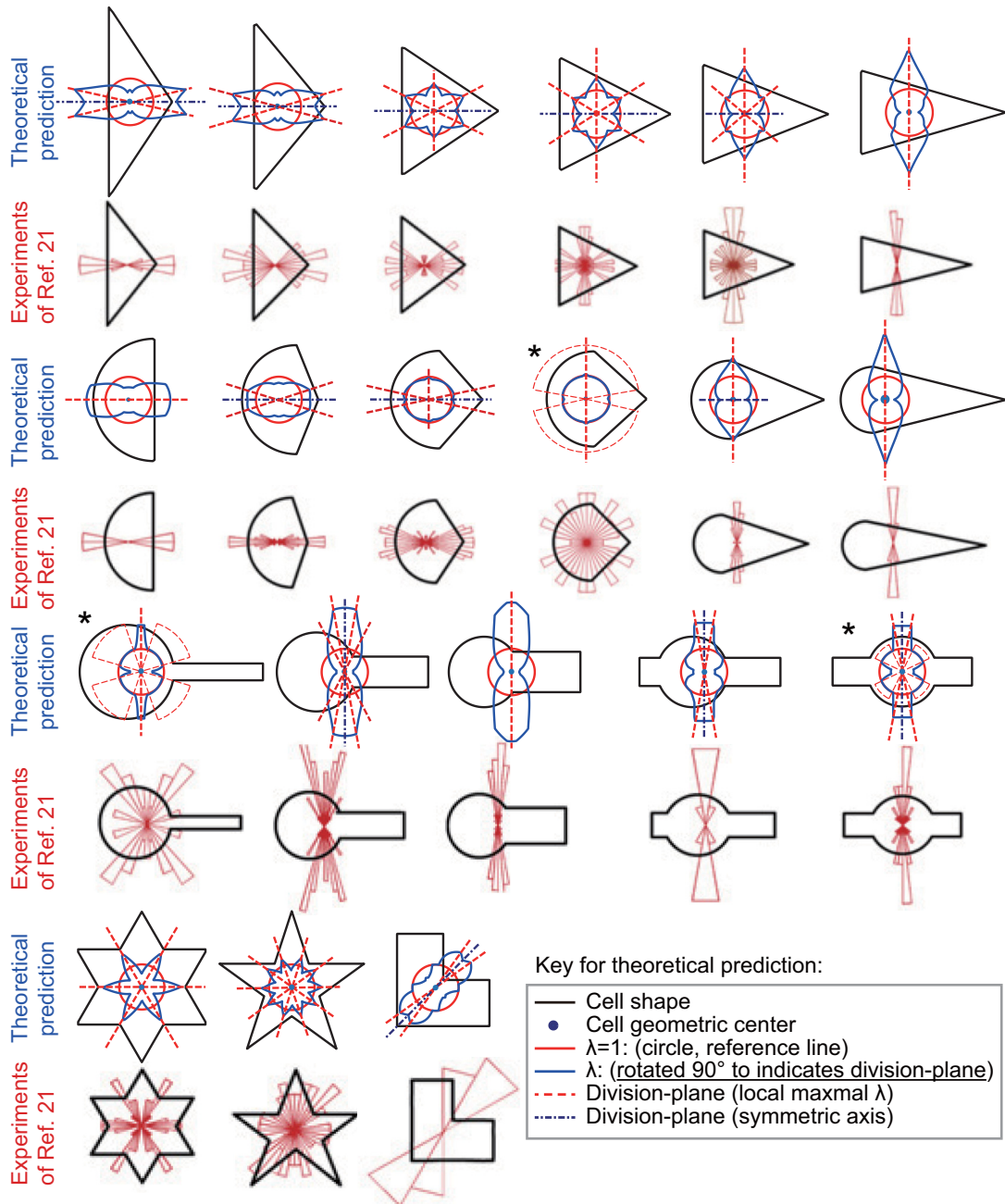


FIG. 7. Comparison of the rule-based predictions with the experiment results in Ref. [21]. Based on the rule of spindle orientation we proposed above [Fig. 6(k)], we plot the radial profile λ (inner blue solid line) of each shape in the polar coordinate system together with the cell shape (black solid line). The radial profile λ has been rotated 90° to indicate the division-axis orientation as the experiments. Experiments results show the spindle tends to orient along the local maximum of λ and $\lambda > 1$ (red dash). If the peak value of λ is bigger, then the probability that the spindle is along this direction can be larger. In the meanwhile, division plane also tends to orientate the symmetric axis of the cell (blue dash). In some shapes (indicated by asterisk), there are some ranges that λ almost keeps constant and equals 1. In this case, the orientation is randomly distributed in these ranges like round or square cells. The experimental results are in good agreement with the prediction of the rule.

of λ (red dash) and $\lambda > 1$. The spindle has a larger probability to orient along the direction with the higher peak value of λ . In the meanwhile, the division axis in some cells also tends to orientate the symmetric axis of the cell (blue dash dot). Besides, in some shapes (indicated by asterisk), there are some ranges that λ almost keeps constant and equals 1. In this case, the orientation can distribute in these ranges randomly like the circle cell or square cell [as in Fig. 6(c)]. Taken together,

since the rule can qualitatively predict the experimental data, we conclude that we propose a general rule and provide a new method to predict the spindle orientation in various cells.

E. Repositioning of the spindle poles during the anaphase

Cells will enter mitotic anaphase after all chromosomes are connected correctly and aligned on the equatorial plate

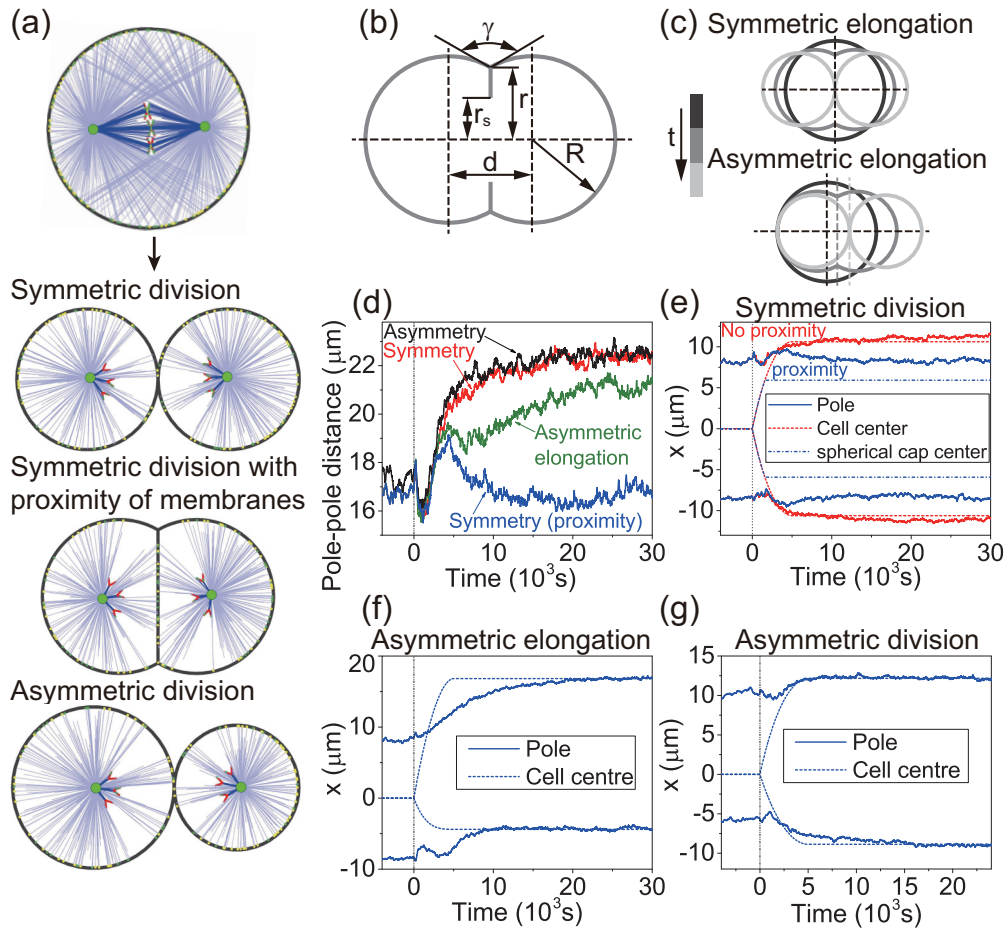


FIG. 8. Simulations of cell division during the mitotic anaphase. (a) Snapshots of simulation results for three cases, including the (1) normal symmetric division (see also Movie 4 in the Supplemental Material [57]); (2) the symmetric division with proximity of the two cell membranes (see also Movie 5 in the Supplemental Material [57]); and (3) the asymmetric division (see also Movie 6 in the Supplemental Material [57]). To achieve the asymmetric division, a higher binding rate of dynein $k_b^+ = 0.06$ on the right half cortex is given to deflect the spindle ($\sim 3\mu\text{m}$). (b) Schematic diagram of the cell shape during the cytoplasmic division. The radius of contractile ring r_s decreases linearly over time. If the cell membranes are not proximate to each other in the division plane, then $r_s \equiv r$. Otherwise, a critical angle $\gamma = 3\pi/2$ is defined as the onset of the proximity, and then r is constant. The volume of the whole cell is assumed constant. (c) Schematic diagrams of symmetric and asymmetric elongation of the cell membrane. (d) The distances between the spindle poles are the functions of time for the four cases. [(e)–(g)] The x coordinates of the spindle poles and the centers of the two spherical caps are the functions of time for the (e) symmetric division, (f) asymmetric elongation, and (g) asymmetric division.

[45]. At the onset of anaphase, the connection between sister kinetochores breaks, and sister chromatids are separated by pulling forces [3]. The contractile ring self-assembles near the equatorial plane, and the cytoplasm gradually divides into two daughter cells. During this process, the spindle poles can be repositioned to the center of the daughter cells [76].

Our model can also be used to study this process through minor modification. First, the change of the cell shape needs to be specified. For simplicity, we assume the cell is round at the beginning of anaphase and then becomes two connected spherical caps due to the contraction of the ring [Figs. 8(a) and 8(b)]. A sequence of cell shapes is used in the simulation, and the cell volume (that is, the cell area in the 2D model) is assumed to be constant. The change of the cell shape can also be easily modified based on the mechanical models [77–81]. Second, at the beginning of anaphase, the connection between each pair of sister kinetochores breaks simultaneously. Then,

the sister chromatids, that is, the two halves of the X-shaped chromosome, are pulled to the two spindle poles. Since the chromatid arms are behind the kinetochore when the chromatid is moving to the spindle pole [63], we assume that the chromatid has a V shape with an angle of 60° [Fig. 8(a)]. The change of the chromatids from the half X shape to the V shape is also represented by a sequence of shapes.

Through these modifications, we can simulate the motions of the spindles during mitotic anaphase (Movies 4–7 in the Supplemental Material [57]). During the cytoplasmic division of animal cells, the round mother cell can be divided into two round daughter cells by the contractile ring [79]. One exception is that due to the geometrical confinement outside the *Caenorhabditis elegans* zygote [77,78,80,82], the membranes of the two daughter cells on the division plane are very proximate so that after cell division the two daughter cells are not round but are two spherical caps [83]. In our simulations,

we consider both cases, the normal symmetric division and the asymmetric division, with the proximity of membranes [Figs. 8(a) and 8(b)]. Furthermore, we also consider two other cases, asymmetric division and asymmetric elongation [Figs. 8(a) and 8(b)]. Asymmetric division occurs when the division plane deviates from the cell center, and the daughter cells have different sizes, which plays an important role in self-renewal and differentiation [8,84]. Asymmetric elongation means that the cell membrane of one daughter cell grows faster than the other, which leads to the shift of the cell center [76]. We assume that when asymmetric elongation occurs, the division is symmetric but the left boundary is fixed [Fig. 8(c)].

Similarly to the experimental results [85,86], we show that the pole-to-pole distance increases with time after the onset of anaphase and finally approaches a stable state in the four cases [Fig. 8(d)]. Our simulation also shows that after the cytoplasmic division the centrosomes can be repositioned to the centers of the daughter cells in all cases without other unspecified mechanisms [Figs. 8(e)–8(g)], which is also consistent with experimental observation [76]. These results show the high applicability and expansibility of our model.

IV. DISCUSSION

In this work, we develop a general model for mitotic spindles (Figs. 1–3) and investigate the positioning and orientation of spindles systematically. How the spindle is positioned in a cell is a fundamental question. Many theoretical and experimental studies [10–19,31,52] have shown that spindles can be centered by the mechanical forces generated by the dynamics of the microtubules and molecular motors. Most of these forces are believed to be length dependent or position dependent, so they can sense the cell boundary and drive the spindle to move to the cell center. Here the question we want to ask is how the spindles are positioned faster and more efficiently in cells with different sizes and shapes. We use the dynamic simulations by considering more complete mechanisms to answer this question. We find that in a given cell, on the premise of successful positioning, the proper distribution and composition of the microtubules can provide a fast and efficient positioning process (Fig. 4). We also find the positioning process slows down with the increase of cell size (Fig. 5). These results are in agreement with the experimental observations that the positioning becomes weaker with the activation of the cortical dynein or in larger cells [69]. Although the characteristic time of positioning increases with the cell size, the combination of cortical and cytoplasmic forces can ensure that the positioning of the spindles is efficient across multiple length scales. The cytoplasmic force makes up for the decrease of the cortical force and turns the fast increase of the characteristic time into a slow linear increase (Fig. 5).

Compared to the positioning, the orientation of the mitotic spindles was relatively less focused. It has been shown that only the length-dependent pulling force on the microtubules can orient the spindles in various cells [21–23]. Here we show that the orientation of the spindles is driven by the torque generated by the positioning of the two spindle poles (Fig. 4). Therefore, both the pulling and pushing forces can drive the orientation of the spindles (Figs. 4 and 5). Interestingly, the orientation of

the spindles also has some specific properties that are different from the positioning. For example, if the cell has a higher aspect ratio, then the orientation process can be faster (Fig. 6), which explains the experimental observation that in a more slender cell, the spindle has a higher probability to be oriented along the major axis [21–23].

Furthermore, we investigate the final orientation of the spindles in polygonal cells. The simulation results of spindle orientation in square cells and rectangular cells are in good agreement with the experimental results by confining the cell in microfabricated chambers [21]. Our model can also simulate any other shape. Here we simulate the spindle orientation in rhombic, pentagonal, and hexagonal cells, but these results still require further experimental verifications. Based on these simulations, we propose a general rule that the spindle orientation is either the local maximum radial profile or the long symmetrical axis (Fig. 6). This rule successfully predicts the division-axis orientation in other cell shapes observed experimentally in Ref. [21] (Fig. 7). Therefore, we provided a new method to qualitatively predict of the spindle orientation in various cells. This method is based only on the cell shape and does not need simulations or solving equations, and thus it is more convenient, quick, and intuitive than our simulations or the previous analytical model [21]. Therefore, we proposed a generalization of the classical long-axis rule.

Based on the framework of our computational model, we can answer many other questions about spindles through minor modifications. In our recent work, we investigated the size regulation of spindles and found that the geometric asymmetry induces the upper limit of the spindle size [28]. Here we also modify the model and simulate the chromosome separation and repositioning of the spindle poles during mitotic anaphase (Fig. 8). We found that the two centrosomes can be separated and repositioned to the center of the daughter cells in the absence of other specified mechanisms, which is in agreement with experimental observations [76,85,86]. In the future, we will also study other factors, such as the mechanical property of spindles and the influence of the cell polarity factor or yolk bias on spindle orientation [34]. Therefore, our model provides an effective tool for studying the mitotic spindle across the whole mitotic phase.

We use the 2D simulation to study the positioning and orientation of spindles, because we have found that the results of 2D and 3D simulations have only quantitative differences, but the 3D simulation requires greater computational cost [28]. However, the 2D simulation has a limitation that the microtubules can barely bypass the chromosomes to form antiparallel structures. Therefore, we only consider the interaction between the antiparallel microtubules implicitly [28]. Therefore, due to the masking of the antiparallel microtubules, the simulation snapshot seems different from the real spindle, especially the anaphase spindle. Three-dimensional simulation can overcome this problem and is an alternative for further applications [28].

We consider more complete mechanisms, and thus our simulation is more realistic than previous computational models and has a wider application as discussed above. Furthermore, we consider only the buckling of microtubules but do not describe the elastic deformation of microtubules in detail as in Refs. [35,36]. After this simplification, the computational

efficiency of our simulations containing thousands of microtubules [87] is increased. Therefore, our model can be more efficient to simulate many phenomena of mitotic spindles. However, more precise microtubule deformation [35,36], and other known phenomena, such as the branching and severing [37,44,88], are simplified or neglected, as in some previous models [18,19]. But they can be considered in the model if necessary in the future.

ACKNOWLEDGMENTS

This work was supported by the National Natural Science Foundation of China (Grants No. 11622222 and No. 11472271), the Thousand Young Talents Program of China, the Fundamental Research Funds for the Central Universities (Grant No. WK2480000001), and the Strategic Priority Research Program of the Chinese Academy of Sciences (Grant No. XDB22040403).

-
- [1] S. L. Kline-Smith and C. E. Walczak, *Mol. Cell* **15**, 317 (2004).
- [2] M. E. Tanenbaum and R. H. Medema, *Dev. Cell* **19**, 797 (2010).
- [3] J. R. McIntosh, M. I. Molodtsov, and F. I. Ataullakhanov, *Q. Rev. Biophys.* **45**, 147 (2012).
- [4] L. Stevermann and D. Liakopoulos, *Curr. Opin. Cell Biol.* **24**, 816 (2012).
- [5] S. Kotak and P. Gönczy, *Curr. Opin. Cell Biol.* **25**, 741 (2013).
- [6] F. J. McNally, *J. Cell. Biol.* **200**, 131 (2013).
- [7] S. Dumont and T. J. Mitchison, *Curr. Biol.* **19**, R749 (2009).
- [8] X. Morin and Y. Bellaïche, *Dev. Cell* **21**, 102 (2011).
- [9] M. Théry and M. Bornens, *Curr. Opin. Cell Biol.* **18**, 648 (2006).
- [10] S. W. Grill and A. A. Hyman, *Dev. Cell* **8**, 461 (2005).
- [11] K. Kimura and A. Kimura, *Proc. Natl. Acad. Sci. U.S.A.* **108**, 137 (2011).
- [12] J. Wu, G. Misra, R. J. Russell, A. J. Ladd, T. P. Lele, and R. B. Dickinson, *Mol. Biol. Cell* **22**, 4834 (2011).
- [13] G. Letort, F. Nédélec, L. Blanchoin, and M. Théry, *Mol. Biol. Cell* **27**, 2833 (2016).
- [14] J. Howard, *Phys. Biol.* **3**, 54 (2006).
- [15] M. Dogterom and B. Yurke, *Phys. Rev. Lett.* **81**, 485 (1998).
- [16] S. Inoué and E. D. Salmon, *Mol. Biol. Cell* **6**, 1619 (1995).
- [17] P. Tran, L. Marsh, V. Doye, S. Inoue, and F. Chang, *J. Cell Biol.* **153**, 397 (2001).
- [18] J. Zhu, A. Burakov, V. Rodionov, and A. Mogilner, *Mol. Biol. Cell* **21**, 4418 (2010).
- [19] N. Pavin, L. Laan, R. Ma, M. Dogterom, and F. Jülicher, *New J. Phys.* **14**, 105025 (2012).
- [20] I. M. Tolić-Nørrelykke, *Eur. Biophys. J.* **37**, 1271 (2008).
- [21] N. Minc, D. Burgess, and F. Chang, *Cell* **144**, 414 (2011).
- [22] M. Théry, A. Jimenez-Dalmaroni, V. Racine, M. Bornens, and F. Jülicher, *Nature* **447**, 493 (2007).
- [23] F. Bosveld, O. Markova, B. Guirao, C. Martin, Z. Wang, A. Pierre, M. Balakireva, I. Gaugue, A. Ainslie, and N. Christophorou, *Nature* **530**, 495 (2016).
- [24] M. Wühr, Y. Chen, S. Dumont, A. C. Groen, D. J. Needleman, A. Salic, and T. J. Mitchison, *Curr. Biol.* **18**, 1256 (2008).
- [25] M. C. Good, M. D. Vahey, A. Skandarajah, D. A. Fletcher, and R. Heald, *Science* **342**, 856 (2013).
- [26] J. Hazel, K. Krutkramelis, P. Mooney, M. Tomschik, K. Gerow, J. Oakey, and J. Gatlin, *Science* **342**, 853 (2013).
- [27] S. Dumont and T. J. Mitchison, *Curr. Biol.* **19**, 1086 (2009).
- [28] J. Li and H. Jiang, *Biophys. J.* **112**, 1503 (2017).
- [29] X. Wan, D. Cimini, L. A. Cameron, and E. Salmon, *Mol. Biol. Cell* **23**, 1035 (2012).
- [30] H. Jiang, *Sci. Rep.* **5**, 10504 (2015).
- [31] L. Laan, N. Pavin, J. Husson, G. Romet-Lemonne, M. Van Duijn, M. P. López, R. D. Vale, F. Jülicher, S. L. Reck-Peterson, and M. Dogterom, *Cell* **148**, 502 (2012).
- [32] F. Xiong, W. Ma, T. W. Hiscock, K. R. Mosaliganti, A. R. Tentner, K. A. Brakke, N. Rannou, A. Gelas, L. Souhait, I. A. Swinburne *et al.*, *Cell* **159**, 415 (2014).
- [33] T. P. Wyatt, A. R. Harris, M. Lam, Q. Cheng, J. Bellis, A. Dimitracopoulos, A. J. Kabla, G. T. Charras, and B. Baum, *Proc. Natl. Acad. Sci. U.S.A.* **112**, 5726 (2015).
- [34] A. Pierre, J. Sallé, M. Wühr, and N. Minc, *Dev. Cell* **39**, 667 (2016).
- [35] F. Nédélec, *J. Cell Biol.* **158**, 1005 (2002).
- [36] W. E. Channels, F. J. Nédélec, Y. Zheng, and P. A. Iglesias, *Biophys. J.* **94**, 2598 (2008).
- [37] R. Loughlin, R. Heald, and F. Nédélec, *J. Cell Biol.* **191**, 1239 (2010).
- [38] G. Goshima, R. Wollman, N. Stuurman, J. M. Scholey, and R. D. Vale, *Curr. Biol.* **15**, 1979 (2005).
- [39] O. Campas and P. Sens, *Phys. Rev. Lett.* **97**, 128102 (2006).
- [40] G. Civelekoglu-Scholey, D. Sharp, A. Mogilner, and J. Scholey, *Biophys. J.* **90**, 3966 (2006).
- [41] E. J. Banigan, K. K. Chiou, E. R. Ballister, A. M. Mayo, M. A. Lampson, and A. J. Liu, *Proc. Natl. Acad. Sci. USA* **112**, 12699 (2015).
- [42] N. Pavin and I. M. Tolić, *Annu. Rev. Biophys.* **45**, 279 (2016).
- [43] K. Ishihara, P. A. Nguyen, A. C. Groen, C. M. Field, and T. J. Mitchison, *Proc. Natl. Acad. Sci. USA* **111**, 17715 (2014).
- [44] S. Petry, A. C. Groen, K. Ishihara, T. J. Mitchison, and R. D. Vale, *Cell* **152**, 768 (2013).
- [45] A. Mogilner and E. Craig, *J. Cell Sci.* **123**, 3435 (2010).
- [46] F. Gittes, B. Mickey, J. Nettleton, and J. Howard, *J. Cell Biol.* **120**, 923 (1993).
- [47] T. E. Holy, M. Dogterom, B. Yurke, and S. Leibler, *Proc. Natl. Acad. Sci. U.S.A.* **94**, 6228 (1997).
- [48] T. Wittmann, A. Hyman, and A. Desai, *Nat. Cell Biol.* **3**, E28 (2001).
- [49] A. Wilde, S. B. Lizarraga, L. Zhang, C. Wiese, N. R. Glikzman, C. E. Walczak, and Y. Zheng, *Nat. Cell Biol.* **3**, 221 (2001).
- [50] S. J. King and T. A. Schroer, *Nat. Cell Biol.* **2**, 20 (2000).
- [51] K. Svoboda and S. M. Block, *Cell* **77**, 773 (1994).
- [52] M. Wühr, E. S. Tan, S. K. Parker, H. W. Detrich, and T. J. Mitchison, *Curr. Biol.* **20**, 2040 (2010).
- [53] J. C. Waters, R. V. Skibbens, and E. D. Salmon, *J. Cell Sci.* **109**, 2823 (1996).
- [54] E. Nazockdast, A. Rahimian, D. Needleman, and M. Shelley, *Mol. Biol. Cell* **28**, 3261 (2017).
- [55] N. J. Nannas, E. T. O'Toole, M. Winey, and A. W. Murray, *Mol. Biol. Cell* **25**, 4034 (2014).
- [56] V. Syrovatkina and P. T. Tran, *Nat. Commun.* **6**, 7322 (2015).

- [57] See Supplemental Material at <http://link.aps.org/supplemental/10.1103/PhysRevE.97.012407>, which includes one figure, seven movies, one table and Refs. [58–62].
- [58] A. P. Joglekar and A. J. Hunt, *Biophys. J.* **83**, 42 (2002).
- [59] T. Gao, R. Blackwell, M. A. Glaser, M. D. Betterton, and M. J. Shelley, *Phys. Rev. Lett.* **114**, 048101 (2015).
- [60] Z. Wang, S. Khan, and M. P. Sheetz, *Biophys. J.* **69**, 2011 (1995).
- [61] S. Toba, T. M. Watanabe, L. Yamaguchi-Okimoto, Y. Y. Toyoshima, and H. Higuchi, *Proc. Natl. Acad. Sci. USA* **103**, 5741 (2006).
- [62] M. Dogterom and B. Yurke, *Science* **278**, 856 (1997).
- [63] J. Maciejowski, Y. Li, N. Bosco, P. J. Campbell, and T. de Lange, *Cell* **163**, 1641 (2015).
- [64] W. T. Silkworth, I. K. Nardi, R. Paul, A. Mogilner, and D. Cimini, *Mol. Biol. Cell* **23**, 401 (2012).
- [65] B. Shtylla and J. P. Keener, *J. Theor. Biol.* **263**, 455 (2010).
- [66] W. T. Gibson, J. H. Veldhuis, B. Rubinstein, H. N. Cartwright, N. Perrimon, G. W. Brodland, R. Nagpal, and M. C. Gibson, *Cell* **144**, 427 (2011).
- [67] C. Faivre-Moskalenko and M. Dogterom, *Proc. Natl. Acad. Sci. U.S.A.* **99**, 16788 (2002).
- [68] V. Magidson, C. B. OConnell, J. Lončarek, R. Paul, A. Mogilner, and A. Khodjakov, *Cell* **146**, 555 (2011).
- [69] C. Garzon-Coral, H. A. Fantana, and J. Howard, *Science* **352**, 1124 (2016).
- [70] N. Li, A. Tourovskaia, and A. Folch, *Crit. Rev. Biomed. Eng.* **31**, 423 (2003).
- [71] S. Huda, D. Pilans, M. Makurath, T. M. Hermans, K. Kandere-Grzybowska, and B. A. Grzybowski, *Adv. Mater. Interfaces* **1**, 1400158 (2014).
- [72] M. Théry, V. Racine, A. Pépin, M. Piel, Y. Chen, J.-B. Sibarita, and M. Bornens, *Nat. Cell Biol.* **7**, 947 (2005).
- [73] A. S. Maddox and K. Burridge, *J. Cell. Biol.* **160**, 255 (2003).
- [74] M. P. Stewart, J. Helenius, Y. Toyoda, S. P. Ramanathan, D. J. Muller, and A. A. Hyman, *Nature* **469**, 226 (2011).
- [75] O. M. Lancaster, M. Le Berre, A. Dimitracopoulos, D. Bonazzi, E. Zlotek-Zlotkiewicz, R. Picone, T. Duke, M. Piel, and B. Baum, *Dev. Cell* **25**, 270 (2013).
- [76] T. Kiyomitsu and I. M. Cheeseman, *Cell* **154**, 391 (2013).
- [77] A. Sain, M. M. Inamdar, and F. Jülicher, *Phys. Rev. Lett.* **114**, 048102 (2015).
- [78] A. S. Maddox, L. Lewellyn, A. Desai, and K. Oegema, *Dev. Cell* **12**, 827 (2007).
- [79] H. Turlier, B. Audoly, J. Prost, and J.-F. Joanny, *Biophys. J.* **106**, 114 (2014).
- [80] H. Koyama, T. Umeda, K. Nakamura, T. Higuchi, and A. Kimura, *PLoS One* **7**, e31607 (2012).
- [81] M. S. Rizvi and S. L. Das, *J. Theor. Biol.* **315**, 139 (2012).
- [82] A. Carvalho, A. Desai, and K. Oegema, *Cell* **137**, 926 (2009).
- [83] H. Bringmann and A. A. Hyman, *Nature* **436**, 731 (2005).
- [84] J. Cheng, A. Tiyaboonchai, Y. M. Yamashita, and A. J. Hunt, *Development* **138**, 831 (2011).
- [85] A. M. Saunders, J. Powers, S. Strome, and W. M. Saxton, *Curr. Biol.* **17**, R453 (2007).
- [86] M. Kwon, S. Morales-Mulia, I. Brust-Mascher, G. C. Rogers, D. J. Sharp, and J. M. Scholey, *Mol. Biol. Cell* **15**, 219 (2004).
- [87] E. O’Toole, G. Greenan, K. I. Lange, M. Srayko, and T. Müller-Reichert, *PLoS One* **7**, e29795 (2012).
- [88] J. Brugués, V. Nuzzo, E. Mazur, and D. J. Needleman, *Cell* **149**, 554 (2012).